applied sciences

MDPI

Article

Calibration of iPad Pro LiDAR Scanning Parameters for the Scanning of Heritage Structures Using Orthogonal Arrays

Edison Atencio [1,*], Andrea Muñoz [2], Fidel Lozano [2], Jesús González-Arteaga [2] and José Antonio Lozano-Galant [2]

[1] School of Civil Engineering, Pontificia Universidad Católica de Valparaíso, Av. Brasil 2147, Valparaíso 2340000, Chile
[2] Department of Civil Engineering, Universidad of Castilla-La Mancha, 13003 Ciudad Real, Spain; andrea.munoz4@alu.uclm.es (A.M.); fidel.lozanogalant@uclm.es (F.L.); jesus.garteaga@uclm.es (J.G.-A.); joseantonio.lozano@uclm.es (J.A.L.-G.)
* Correspondence: edison.atencio@pucv.cl

Abstract: The deterioration of historical heritage has underscored the need for precise documentation and accurate measurements in restoration and conservation efforts. Detailed documentation not only enhances understanding but also provides architects and engineers with the necessary tools to optimize these processes. However, limited funding has prompted researchers to develop low-cost geomatic tools and methodologies, such as multi-image photogrammetry, to generate 3D point clouds. Technologies like miniaturized Light Detection and Ranging (LiDAR) sensors, integrated into Apple devices such as the iPhone and iPad since 2020, have made these tools more accessible. These sensors deliver direct time-of-flight measurements, enabling accurate 3D data acquisition of historical structures. Despite the critical role that scan parameters—such as scanning speed, sensor angle, lighting, or the distance from the scanned object—may play, there is a lack of detailed studies examining their effects in the literature. To address this gap, this paper employs Taguchi's orthogonal arrays to define the optimal scan parameters for the LiDAR sensor on the 2022 iPad Pro. The optimized parameters are then used to scan a historical building.

Keywords: LiDAR; photogrammetry; iPad Pro; orthogonal arrays; heritage structure; scan parameters

check for updates

Citation: Atencio, E.; Muñoz, A.; Lozano, F.; González-Arteaga, J.; Lozano-Galant, J.A. Calibration of iPad Pro LiDAR Scanning Parameters for the Scanning of Heritage Structures Using Orthogonal Arrays. *Appl. Sci.* **2024**, *14*, 11814. https://doi.org/10.3390/app142411814

Academic Editor: Pedro Couto

Received: 4 November 2024
Revised: 3 December 2024
Accepted: 14 December 2024
Published: 18 December 2024

Copyright: © 2024 by the authors. Licensee MDPI, Basel, Switzerland. This article is an open access article distributed under the terms and conditions of the Creative Commons Attribution (CC BY) license (https://creativecommons.org/licenses/by/4.0/).

1. Introduction

The importance of documentation and metric knowledge in the field of cultural heritage takes on critical relevance when considering the alarming degradation affecting much of the built historical legacy [1], coupled with the necessary interventions for its restoration and conservation. In this context, the meticulous documentation of these valuable structures not only enhances understanding but also provides architects and engineers with the necessary tools to optimize the processes of restoration, safeguarding, and improvement of these cultural treasures [2].

However, a challenge has arisen due to the funding accessibility of these investigations [3]. This situation has catalyzed the creativity and commitment of stakeholders and researchers, who have focused their efforts on creating low-cost geomatic tools and methodologies, without compromising metric accuracy [4]. Among these solutions, multi-image photogrammetry stands out as an effective technique that democratizes the process of metric documentation, encouraging the participation of individuals with no prior geomatic experience [5].

Through the application of multi-image photogrammetry, comprehensive 3D metric surveys can be obtained with a fast and intuitive approach [6]. This technique has versatile applications, ranging from the architectural field to the monitoring of structures and environmental assessment [6]. Specifically, algorithms based on structure-from-motion (SfM) and integrated into multi-image photogrammetry allow for the generation of precise and consistent point clouds, highlighting their suitability for metric documentation [7].

Technological evolution has further facilitated the metric documentation landscape with the introduction of miniaturized and affordable LiDAR (Light Detection And Ranging) sensors [8]. These sensors, such as those integrated into Apple devices since 2020, like the iPhone 12 Pro and the iPad Pro, have popularized the acquisition of 3D data for buildings and historical–cultural heritage assets [9]. This LiDAR, unlike traditional sensors, offers direct time-of-flight measurements (dToF), eliminating mechanical components and ensuring accurate and reliable measurements [10].

To fully harness this advancement, specific applications available in the Apple App Store are required. These applications allow for the acquisition and export of point clouds and meshes in various formats [11]. Both free and paid versions, with more advanced features oriented towards metric documentation, are available [12].

Since the integration of LiDAR into Apple devices, various applications and research groups have explored its geomatic potential and practical applications. Nevertheless, despite the critical role that scan parameters—such as scanning speed, sensor angle, lighting, or the distance from the scanned object—may play, there is a lack of detailed studies examining their effects in the literature. To address this gap, this paper employs Taguchi's orthogonal arrays to define the optimal scan parameters for the LiDAR sensor on the 2022 iPad Pro. Through this initiative, efficient practices for performing scans can be established that yield useful results, raising the question of which parameters influence scan quality and what the optimal levels are for each [4]. The optimized parameters are then used to scan a historical building.

The remining paper is structured as follows. In Section 2, the background of this research is presented in order to summarize the current knowledge in the usage of the iPad for structures scanning. Section 3 comprises the stages, activities, tools and deliverables of the research method conducting this work. A methodology for selecting the optimal levels of scanning parameters for the iPad Pro (Apple Inc., Cupertino, CA, USA), using orthogonal arrays, is also presented. In Section 4, this methodology is applied to three objects with different geometries to determine the ideal scanning parameters. These parameters are then used in Section 5 to monitor the façade of a heritage structure. Discussions of the results are presented in Section 6 and, the conclusions, limitations, and future research of this work are summarized in Section 7.

2. Background

2.1. Heritage Structures Inspection Protocols

Historical constructions face a unique set of challenges due to their age, architectural design, and building materials, as well as the effects of environmental changes and long-term wear. According to [13], one of the primary issues is the degradation of materials. Materials such as stone, wood, and lime mortar, commonly used in historical structures, are prone to deterioration over time. This is primarily caused by exposure to climatic factors, temperature fluctuations, humidity, and atmospheric pollutants, leading to decomposition, erosion, and corrosion. Additionally, historical buildings often experience settling and structural movement over the years, which can result from changes in soil conditions, vibrations from nearby traffic, or other external influences, causing cracks and deformations in the structure [14].

Biological attacks and biodeterioration also pose significant threats, as organisms like fungi, lichens, mosses, and insects can colonize and damage the surfaces of these structures, accelerating the deterioration of materials and affecting their overall appearance. Water-related issues are another major concern. Water infiltration through roofs, walls, and foundations can lead to severe damage, including material degradation and mold formation. Moreover, water can contribute to the erosion and corrosion of structural elements [15].

Another problem arises from the use of modern materials in repairs and restorations, which may be incompatible with the original materials of the historical buildings. This mismatch can lead to further long-term damage. Lastly, many historical constructions do not comply with modern building codes and safety regulations. Adapting these structures

to meet current safety standards and new usage requirements can be complex, often requiring careful consideration to avoid compromising their historical integrity [16].

For the inspection and conservation of historical buildings, various levels of inspection are employed to ensure the proper preservation of their cultural, architectural, and historical value [8]. These include superficial inspections conducted by conservation staff with basic evaluation knowledge but without specialized training in infrastructure pathologies. The main goal of these inspections is to identify visible damage and document it in a report. Visual inspections are carried out by technicians with some training in infrastructure inspection, without the need for special equipment, focusing on detecting visible damage from the ground to assess the general condition of the structure [17].

Main inspections involve close visual evaluations of all parts of the structure, including the ability to physically touch elements during the inspection. Deep inspections are performed during repair work and involve detailed measurements to determine the cause and extent of detected damage, providing precise information for rehabilitation planning. Special inspections are conducted in specific situations or when previous inspections raise particular concerns that require more focused investigation [18].

Several common protocols fall within these inspection levels, as described by [19,20]. The most basic and essential method is visual inspection, which involves a direct assessment of the structure to identify visible damage, deterioration, cracks, humidity, and other surface issues such as paint detachment. Non-destructive techniques allow for the evaluation of the internal state of the structure without causing physical damage, using methods like ultrasound, thermography, electrical resistivity tomography, ground-penetrating radar (GPR), and X-rays. Material analysis involves studying the construction materials of the historical structure, often through laboratory testing, to determine their composition and characteristics, aiding in conservation efforts.

In some cases, continuous monitoring systems are implemented to track changes in the structure over time, using sensors to measure humidity, temperature, vibration, and other factors that could affect the building's integrity [21]. 3D modeling and scanning technologies enable the creation of accurate digital representations of the structure, which are useful for restoration planning and identifying hidden issues.

Historical and documentary research is another critical aspect, providing valuable insights into the original construction methods, alterations over time, and significant events related to the structure [22]. This knowledge informs decisions about conservation. Construction pathology studies focus on identifying the underlying causes of deterioration and damage, whether from design flaws, natural aging, or human intervention.

It is essential to recognize that each historical building is unique, requiring a tailored approach based on its historical context, current condition, and conservation needs [23]. Professionals specializing in historical preservation, such as architects, structural engineers, and conservators, typically use a combination of these protocols to ensure the proper conservation of these invaluable structures. Among the key procedures for inspection and subsequent conservation, monitoring and 3D scanning and modeling stand out, as these techniques contribute significantly to the digitalization of cultural heritage [23].

2.2. iPad Pro LiDAR

Numerous studies have evaluated the use of Apple's iPad Pro LiDAR in heritage conservation and architectural documentation. While its cost-effectiveness and portability make it a promising tool for rapid surveys, its accuracy is consistently found to be lower compared to professional-grade devices like photogrammetry and terrestrial laser scanners (TLS).

Vacca [24] highlighted the sensor's suitability for simpler geometries but noted limitations in range (up to 5 m) and difficulty capturing fine details. Similarly, Łabędź et al. [10] found significant inaccuracies in small, complex objects, with up to 50% of points misaligned, though the sensor performed well in simplifying larger architectural features like walls and facades. Teppati Losè et al. [9] emphasized its usability for preliminary surveys but underlined its reduced precision compared to TLS, making it better suited for broader

heritage documentation tasks. Costantino et al. [24] identified challenges such as surface splitting and inertial navigation drift, highlighting the need for improved calibration to address movement-induced errors.

Díaz-Vilariño et al. [25] pointed out that the reduced range and point density of the iPad Pro's LiDAR limit its suitability for detailed documentation, while Vogt et al. [26] demonstrated its adequacy for basic applications but not for highly detailed scans. Spreafico et al. [11] assessed its positional accuracy, finding it appropriate for mapping at a scale of 1:200 but with noticeable noise in point clouds.

While these studies demonstrate the potential of Apple's LiDAR sensor (Lumentum, San Jose, CA, USA) in heritage documentation, they reveal several limitations:

- Accuracy and Precision: The iPad Pro LiDAR sensor struggles with complex geometries and fine details, particularly when compared to photogrammetry or professional TLS. Calibration techniques specific to the sensor are limited, creating a need for more sophisticated methods to enhance precision in scanning heritage structures.
- Limited Range and Data Density: The LiDAR's range is restricted to 5 m, which limits its usability in larger or taller heritage buildings. The reduced point density also affects the quality of the 3D models produced.
- Error Mitigation in Field Scans: Drift issues and surface splitting in mobile scans have been identified, but robust solutions to mitigate these errors during fieldwork are still lacking.

In addition, the 3D model development quality depends on a set of parameters to be controlled during the capture process [27]. Following the 3D accuracy modeling analysis developed by Atencio et al. [5] the main parameter for 3D modeling to be considered is the distance to the object. Other parameters considered for the model developing include: sensor angle, scanning time, number of passes, lighting, and scanning resolution. These parameters are summarized in Table 1 with the addition of the type of material of the scanned object and the software used for model processing in the main works in the literature.

Table 1. Key parameters considered in the literature.

Reference	Distance to Object	Sensor Angle	Scanning Time	Number of Passes	Lighting	Resolution
[28]	5 m	Varied	Not specified	Not specified	Not specified	1–2 cm
[10]	5 m	Multiple	Not specified	Several	Standard conditions	2 cm
[9]	5 m	Multiple	Not specified	Multiple	Mixed lighting	2–3 cm
[24]	≤3 m	Varied	Not specified	Repeated	Not discussed	1–3 cm
[25]	300 mm–5 m	65°	Not specified	Multiple	Good in low light	2 cm
[26]	5 m	Varied	Not specified	Multiple	Standard lighting	0.05 mm to 0.1 mm
[29]	Not specified	Not specified	Not specified	Not mentioned	Not specified	Not specified
[11]	1–4 m	Perpendicular (varied)	4–20 min	Multiple	Diffuse indoor and natural outdoor	1 cm (max detail high) to 5.2 cm (low)

The analysis of Table 1 shows that the distance to the object generally ranges from 1 to 5 m, which is the typical maximum range for these devices. Sensor angles present a significant variation in the literature, but most studies adopt perpendicular or varied angles to ensure better data capture. Scanning times fluctuate significantly, from a few minutes (around 4 min for lower resolution) to up to 20 min for higher resolution scans with multiple passes. Lighting is generally not a major limiting factor, with scans performed in both natural outdoor and controlled indoor environments. Resolution varies from 1 cm for high-detail settings to as low as 5.2 cm for less detailed scans, with most studies achieving a precision of around 1–2 cm, suitable for applications like architectural surveys. The common thread of the summarized works is the promise of portable, low-cost, and efficient scanning with accuracy close to professional-grade tools in ideal conditions. To identify

the key scanning parameters affecting the iPad Pro LiDAR scanning process, a design for experiments methodology based on Taguchi's orthogonal arrays, as introduced in the following section, was utilized.

It is important to highlight that the iPad Pro's "LiDAR Scanner" is often misunderstood because, while it shares a name with traditional LiDAR systems, its function and capabilities differ. Unlike full-scale LiDAR systems used in applications such as self-driving cars or large-scale surveying, the iPad Pro's LiDAR uses time-of-flight (ToF) technology, which works by measuring the time it takes for a light pulse to travel to an object and return. While this is a form of distance measurement that can be used in 3D scanning, it lacks the depth and range of professional LiDAR scanners, making it a less advanced and more limited implementation. In professional LiDAR systems, lasers are typically used to emit precise light pulses to generate highly detailed 3D models of large areas. These systems are much more powerful, accurate, and capable of scanning over longer distances, whereas the iPad's LiDAR is optimized for short-range applications, mainly used for enhancing augmented reality (AR) experiences, improving focus, and enabling precise measurements within a limited range. Therefore, while Apple's device is marketed as a "LiDAR Scanner", it technically does not match the traditional LiDAR technology in terms of its operational scope or technical capacity, and its usage is more akin to a depth-sensing camera.

2.3. Experiments Design

The Design of Experiments (DoE) theory seeks to reduce the number of simulations while maintaining statistical significance [30]. In the 1960s, Taguchi introduced a set of tables (known as orthogonal arrays) to minimize experiments required for statistically significant results [31]. This method helps researchers understand the relationship between process factors and outcomes [13] and has been applied across various fields, including agriculture, materials science, and civil engineering. Among the various applications in civil engineering, it is important to highlight the use of Taguchi's method to calibrate the parameters of heuristic optimization tools in the analysis of the tensioning of cable-stayed bridges [32], and for the calibration of the Unmanned Aerial Vehicles (UAV) flight parameters for building façades [4] and road potholes [5,27]

3. Research Method

The research outlined in this document follows the Design Science Research Methodology (DSRM), which aims to develop an artifact that solves a specific problem within a particular context [33]. Examples of the application of this methodology can be found in [34–36] where various problems have been addressed through the development of artifacts that have been tested as both conceptual and practical solutions in real-world scenarios.

Figure 1 represents a step-by-step process based on the DSRM applied to the development and evaluation of a 3D modeling workflow using an iPad Pro LiDAR sensor for scanning structures. This figure includes the stages, objectives, activities, and tools comprising the DSRM adaptation for the present research, aiming to calibrate the scanning parameters for the 3D model using iPad Pro LiDAR sensors.

The analysis of Figure 1 illustrates that the process starts with Stage 1: Identification of problems, where current applications and scanning parameters for the LiDAR sensor are identified through a literature review. In Stage 2: Definition of the potential solution, the parameters for scanning are calibrated, and the workflow is designed, including sensor configurations and scanning methods. Stage 3: Design and development involves refining the scanning setup and determining software for image data processing. Stage 4: Demonstration applies the proposed workflow, capturing data using the iPad Pro LiDAR and generating 3D models, while extracting geometric properties of selected objects. Finally, Stage 5: Evaluation uses statistical analysis to compare the accuracy of the experimental results, applying an Analysis of Variance (ANOVA) to assess the significance of errors and refine the process based on these findings. Each stage is associated with specific tools and activities to ensure the development of an effective 3D modeling solution.

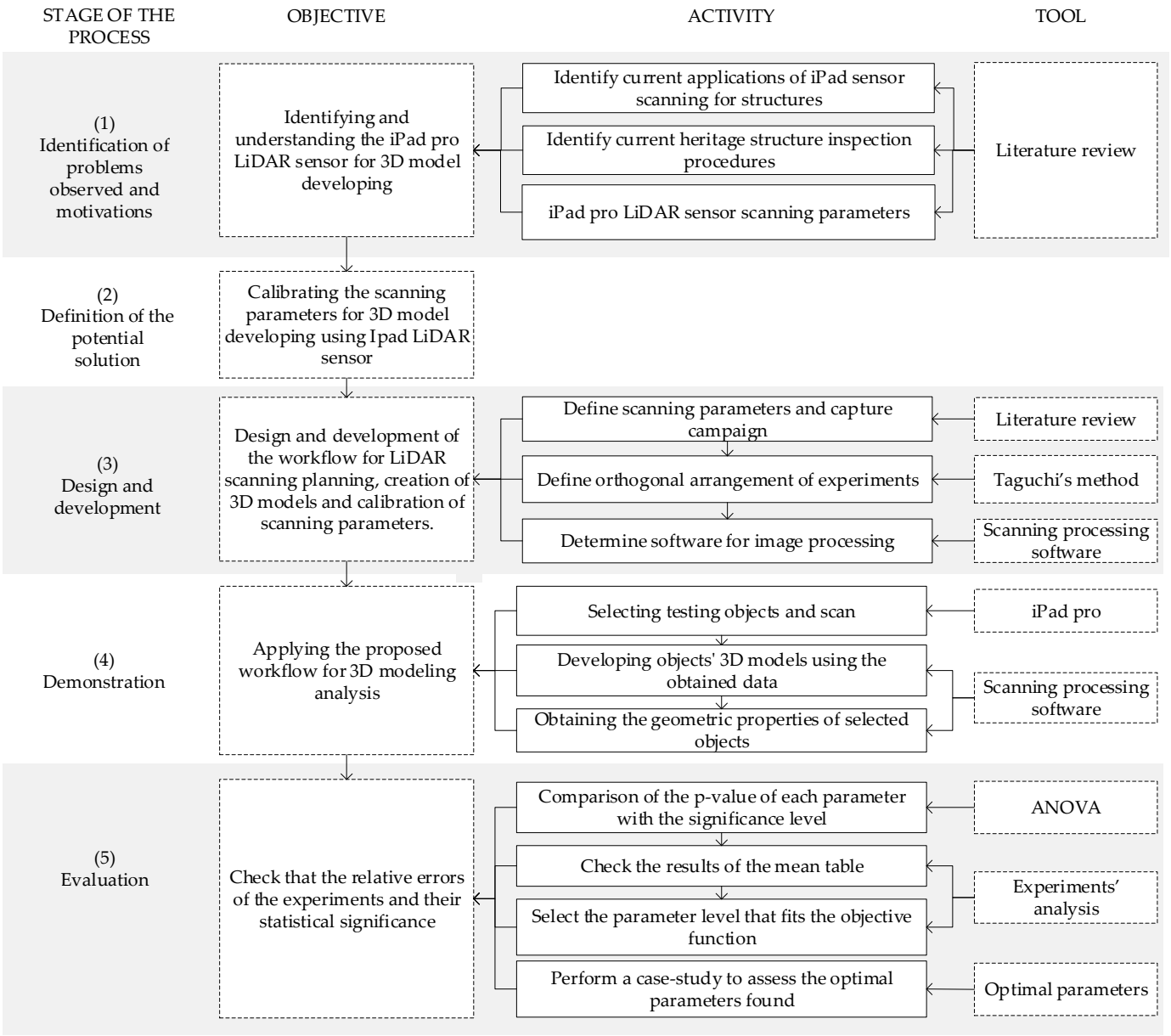


Figure 1. Research method.

Finally, a case study will be conducted to apply the optimal parameters identified in a real-world scenario and evaluate the model's performance. This evaluation will compare the model (using these optimal parameters) against other models developed with randomly assigned parameters. The comparison will be based on error analysis.

4. Results

This section seeks to address stages three, four and five of DSRM presented in Figure 1.

To select the optimal levels for the iPad Pro LiDAR scanning parameters, three objects with different geometries were chosen as calibration targets. These objects are as follows:

1. Parallelepiped Game Box (featuring a simple geometry): This object is a rectangular parallelepiped with six rectangular faces and right angles, representing one of the simplest scanned geometries. It was selected to provide reference measurements in a clear and straightforward manner. In addition, it is important to highlight that this object has no significant color variations across its faces, as all are uniformly white. The dimensions of this object are: Length (a) = 35.4 cm, Depth (b) = 25 cm,

Height (c) = 5.7 cm. These dimensions were used to calculate the object volume resulting in a value of Volume (V) = 5044.50 cm^3. Figure 2a shows an image of this object with its corresponding dimensions.

2. Block of Cubes (featuring different colors in simple geometries): This object consists of three Rubik's cubes assembled in a block, each with a different size (l) and volume (V). Its dimensions are as follows: Cube 1: l_1 = 5.2 cm, V_1 = 140.61 cm^3; Cube 2: l_2 = 5.6 cm, V_2 = 175.62 cm^3; and Cube 3: l_3 = 5 cm, V_3 = 125.00 cm^3. The total volume (V_{total}) is 5845.72 cm^3. This object was selected to examine the effects of different colors on the performance of the scanning device. It is important to highlight that this feature could be beneficial for scanning or measurement techniques that rely on light reflection, such as LiDAR, as the variety of surfaces generates richer and more varied data. A picture of the object is presented in Figure 2b.
3. Sculpture (featuring complex geometries): This object is a Buddha sculpture (Figure 2c), selected for its complexity, as unlike the previous two objects, it does not have flat faces. For measurements, the height of the sculpture and two additional reference dimensions marked by specific points were considered. Additionally, its volume was measured using Archimedes' principle by observing the volume of water displaced by the object. The dimensions are as follows: Height (h) = 19.8 cm, Measurement 1 (m_1) = 12.6 cm, Measurement 2 (m_2) = 2.1 cm, and Volume (V) = 360 cm^3. A photo of this object is shown in Figure 2 together with its considered measurements.

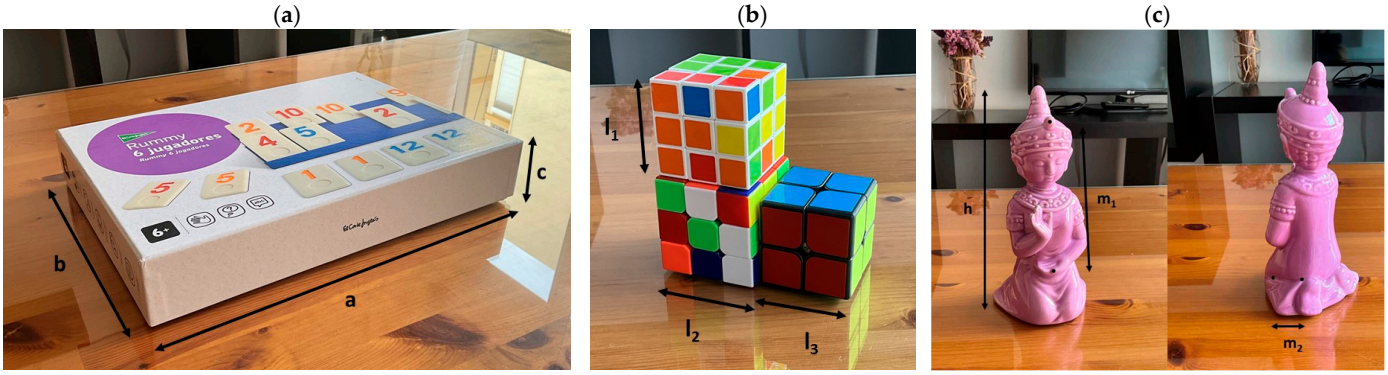


Figure 2. Studied objects: (**a**) Parallelepiped Game Box, (**b**) Block of Kubik's cubes, and (**c**) Buddha shape sculpture.

For the experimental design, five modeling parameters were considered for each of the three objects. Based on parameter values from related studies (summarized in Table 1), three levels were defined for each parameter:

- Distance to Object: 0.5 m, 1.0 m, and 4.0 m.
- Scanning Speed: slow (0.38 m/s), medium (0.7 m/s), and fast (1.26 m/s).
- Sensor Angle: 0°, 30°, and variable (greater than 30°).
- Environmental Lighting:
    - Natural: ambient daylight.
    - Artificial with Low Light: four 35 W light bulbs placed 2.5 m away (Figure 3a).
    - Artificial with High Light: four 35 W light bulbs at 3 m, plus a 15 W bulb positioned 60 cm from the object (Figure 3b).
- Number of Scanning Passes: 1, 2, and 4.

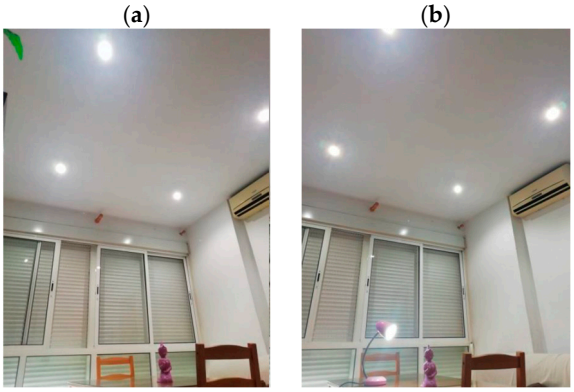


Figure 3. Artificial light with low (**a**) and high light (**b**).

The combination of each parameter and their levels results in 3^5 (243) experiments. To reduce this number, Taguchi's orthogonal arrays were employed. Specifically, we used the L18 array, which allows for the analysis of up to one parameter at two levels and seven parameters at three levels, requiring only 18 tests. The application of the L18 array to the study of the scanning parameters for the analysis of the three objects is summarized in Table 2.

Table 2. Application of the L18 array to the study of the scanning parameters.

Experiment Number	Distance [m]	Speed	Sensor Angle [deg]	Lighting	Number of Passes
1	0.5	Slow	0	Natural	1
2	0.5	Medium	30	Artificial Low	2
3	0.5	Fast	Variable	Artificial High	4
4	1	Slow	0	Artificial Low	2
5	1	Medium	30	Artificial High	4
6	1	Fast	Variable	Natural	1
7	4	Slow	30	Natural	4
8	4	Medium	Variable	Artificial Low	1
9	4	Fast	0	Artificial High	2
10	0.5	Slow	Variable	Artificial High	2
11	0.5	Medium	0	Natural	4
12	0.5	Fast	30	Artificial Low	1
13	1	Slow	30	Artificial 2	1
14	1	Medium	Variable	Natural	2
15	1	Fast	0	Artificial 1	4
16	4	Slow	Variable	Artificial 1	4
17	4	Medium	0	Artificial 2	1
18	4	Fast	30	Natural	2

Table 3 presents a comparative analysis of the main characteristics of three free state-of-the-art LiDAR applications: Polycam (https://poly.cam/, accessed on 3 December 2024), Scaniverse (https://scaniverse.com/, accessed on 3 December 2024), and 3D Scanner App (https://3dscannerapp.com/, accessed on 3 December 2024). The table outlines their pros, cons, suitable use cases, and supported platforms, based on authors' experience.

Table 3. Comparative analysis of LiDAR applications.

Tool	Pros	Cons	Best Use Case	Platform
Polycam	High-quality 3D scans with detailed textures. Supports both LiDAR and photogrammetry modes. Cloud processing for advanced editing and sharing	Heavier on device processing power.	Professional use: architecture, engineering, and design fields.	iOS, Android, and Web.
Scaniverse	User-friendly interface, great for beginners. Produces high-quality 3D models.	Lacks some advanced editing features. No direct cloud processing for large models.	Beginners or casual users needing quick, decent-quality scans.	iOS only.
3D Scanner App	Compatible with LiDAR and ARKit-enabled devices. High precision and reliable outputs. Allows for easy export in various formats (e.g., OBJ, STL).	Interface can feel less intuitive compared to Scaniverse. Requires a strong learning curve for advanced functionalities.	Ideal for detailed LiDAR scans for technical and creative projects.	iOS only.

Polycam was selected over Scaniverse and 3D Scanner App due to its versatility, high-quality output, and suitability for professional applications [37]. It offers both LiDAR scanning and photogrammetry, providing a broader range of scanning options and ensuring high-resolution 3D models with detailed textures, which are essential for architectural and engineering studies. Polycam's advanced editing and cloud processing features allow for efficient model sharing and collaboration, a crucial aspect for research workflows. Additionally, it is compatible with iOS, Android, and web platforms, offering greater flexibility compared to the iOS-only Scaniverse and 3D Scanner App. While Scaniverse is user-friendly and free, it lacks the advanced features required for the study, and 3D Scanner App, although precise, has a steeper learning curve and is limited to LiDAR functionality. Thus, Polycam's comprehensive feature set and proven performance in professional settings made it the most suitable choice for this research.

Each of the three objects was scanned using the 18 parameter configurations defined in Table 2. In each experiment, a mesh of the scanned object was generated to measure both its targeted dimensions and its volume as a solid. The chosen software for this purpose was iTwin Capture Modeler Master [38], and the scanned objects were exported in the '.PLY' format.

To measure the dimensions and the volume of the scanned objects, the scanned mesh was first converted into a solid. This involved importing the mesh into a block that could be imported into the iTwin Capture Desktop Viewer for measurement. An example of the use of this software for the measurement of the length, and the volume in the analyzed objects is presented in Figures 4a and 4b, respectively.

Issues arose during the volume measurement of the mesh, leading to concerns about the accuracy of the data. The measurement process was not conducted in a well-defined manner, making the resulting data unrepresentative. As a result, it was decided to work exclusively with the length data. Accordingly, measurements for each of the three objects were obtained across the 18 experiments defined in Table 2. After that, the relative error of each of these measurements was calculated, and an average of the errors for each experiment was computed.

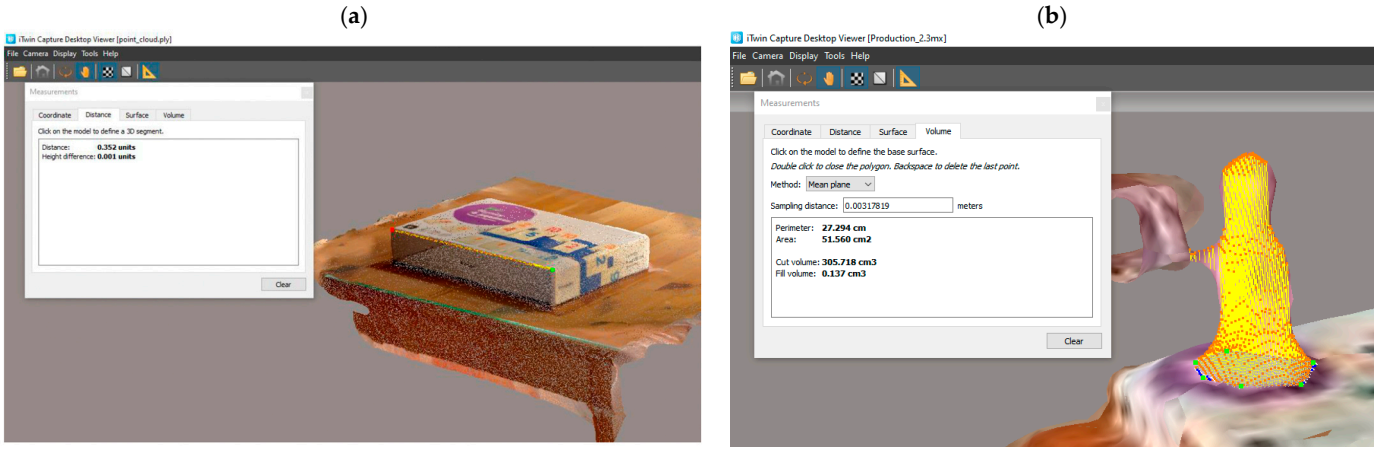


Figure 4. Measurement of length (**a**) and volume (**b**) in the objects imported into iTwin Capture Desktop software (https://www.bentley.com/software/itwin-platform/, accessed on 3 November 2024).

To illustrate this process, its application to Experiment 1 using the parallelepiped game box is presented. The sides of this structure, labeled as a, b, and c in Figure 3a, have real measurements of 35.4 cm, 25.0 cm, and 5.7 cm, respectively. For each of these measurements, the relative error, E_r, was calculated using the following equation:

$$E_r = \frac{|M_R - M_M|}{M_R} \quad (1)$$

in which M_R represents the real measurement and M_M the measured value.

The values of the obtained M_M for each of the sides of the structure and the obtained errors for the Experiment 1 are summarized in Table 4. Analysis of this table shows that the errors for this experiment range from 1.6% on side b to 6.2% on side a.

Table 4. Calculation of relative errors in Experiment 1.

Experiment 1	a	b	c
M_R	35.4 cm	25.0 cm	5.7 cm
M_M	33.2 cm	24.6 cm	6.0 cm
E_r	6.2%	1.6%	5.3%

Therefore, it can be noted that the observed measurement error between the game box and its models is 6.2%, 1.6% and 5.3%, respectively.

In order to summarize these found errors in an overall error, the term E_o (representing the overall error) has been defined. This value was calculated by averaging the absolute values of errors (E_r, from Table 3) as shown in the following equation:

$$E_o = \frac{|E_{R,a}| + |E_{R,b}| + |E_{R,c}|}{3} \quad (2)$$

in which, $E_{R,a}$, $E_{R,b}$, and $E_{R,c}$ represent the relative errors in sides a, b, and c, respectively. Therefore, considering the example presented above, the value of E_o for the Experiment 1 was 6.4%.

The E_o for the three objects described in Figure 3 is summarized in Table 5.

To analyze the variance of the errors, the obtained E_o values for each experiment described in Table 4 were introduced into the MINITAB program (https://www.minitab.com/es-mx/, accessed on 3 November 2024) [39], and an ANOVA analysis was conducted. The *p*-value obtained by this analysis enabled the identification of the scanning parameters with statistical significance. Finally, the optimal level of statistical significance for the scan-

ning parameters was identified by analyzing the effects of the different mean standardized values of each parameter level on E_o.

Table 5. Obtained Overall Errors, E_o.

E_0	Object 1	Object 2	Object 3
1	0.063593	0.385156	0.05291
2	0.043593	0.54815	0.096861
3	0.05896	0.465305	0.092714
4	0.011339	0.081612	0.594757
5	0.075553	1.377292	0.123377
6	0.08775	0.909122	0.212843
7	0.187202	0.308509	0.431883
8	0.235664	0.411172	0.549062
9	0.455563	0.299927	0.893216
10	0.063043	0.121557	0.121212
11	0.017676	0.061612	0.01612
12	0.075131	1.104652	0.210197
13	0.105109	0.263645	0.143338
14	0.017029	0.02544	0.147427
15	0.044463	0.220916	0.135883
16	0.255236	0.411172	0.367484
17	0.333517	0.444412	0.249154
18	0.394528	0.546468	0.243146

The ANOVA analysis of the parallelepiped game box is summarized in Table 6. This table includes the number of degrees of freedom, DF, the adjusted sum of squares, Adj SS, the adjusted mean squared, Adj MS, the ratio of the variance between the groups to the variance within the groups, F-value, and the probability of observing the data, or something more extreme, assuming that the null hypothesis (all means are equal) is true in accordance with the *p*-value. The analysis of this table shows that in this object the distance to the object, the speed, and the lighting conditions are statistically significant as their *p*-values are lower than the reference value of 0.05. On the contrary, both the sensor angle and the number of passes do not have a statistically significant impact on the means of the experiments; in other words, they are not statistically representative.

Table 6. Results of the ANOVA for the parallelepiped game box.

	DF	Adj SS	Adj MS	*F*-Value	*p*-Value
Distance	2	0.26367	0.13183	85.22	0.000
Speed	2	0.02007	0.01003	6.49	0.025
Sensor angle	2	0.00349	0.00174	1.13	0.376
Lighting	2	0.01704	0.00852	5.51	0.037
Number of passes	2	0.01050	0.00525	3.39	0.093

To identify the optimal levels among the three analyzed scanning parameters that are statistically significant, a Taguchi analysis was conducted, focusing on the lowest error for each significant parameter level. For the parallelepiped game box, the distance with the lowest error corresponds to level 1, which is 0.5 m. The sensor speed that yielded the lowest error is level 3, which represents the slow speed. Finally, the optimal lighting condition is

level 1, which is artificial low lighting. The effects of the different levels of the statistically significant scanning parameters in the errors are summarized in Table 7.

Table 7. Analysis of the levels of the parameters in the parallelepiped game box.

Level	Distance	Speed	Lighting
1	0.0503	0.1860	0.1109
2	0.0568	0.1205	0.1819
3	0.3102	0.1109	0.1246

The ANOVA analysis of the Rubik's cube block is summarized in Table 8. This analysis reveals that, unlike the parallelepiped game box, none of the scanning parameters were statistically significant, as all *p*-values exceeded 0.05. Table 9 provides a summary of how the various levels of the different scanning parameters impact the errors in the analysis of this object.

Table 8. Results of the ANOVA for the Rubik's cubes block.

	DF	Adj SS	Adj MS	*F*-Value	*p*-Value
Distance to object	2	0.01751	0.00875	0.07	0.935
Speed	2	0.33558	0.16779	1.29	0.332
Sensor angle	2	0.61278	0.30638	2.36	0.164
Lighting	2	0.04846	0.02423	0.19	0.834
Number of passes	2	0.30761	0.15380	1.19	0.361

Table 9. Analysis of the levels of the parameters in the Rubik's cubes block.

Level	Distance	Speed	Sensor Angle	Lighting	Passes
1	0.4477	0.5911	0.2489	0.4629	0.5864
2	0.4797	0.4781	0.6915	0.4954	0.2705
3	0.4036	0.2619	0.3906	0.3727	0.4741

Finally, the results of the ANOVA analysis for the Buddha figure are summarized in Table 10. This analysis indicates that the only statistically significant scanning parameter for this object was the distance to the object, with a *p*-value of 0.043, which is less than 0.05. This parameter is highlighted in bold in the table. This parameter is highlighted in bold in the table. Additionally, Table 11 provides a summary of how the different distance levels affect measurement errors for this object. The analysis shows that, similar to the parallelepiped game box, the optimal distance level is the first one, 0.5 m.

Table 10. Results of the ANOVA for the Buddha figure.

	DF	Adj SS	Adj MS	*F*-Value	*p*-Value
Distance	2	0.3933	0.1966	5.09	0.043
Speed	2	0.0363	0.0181	0.47	0.643
Sensor angle	2	0.0412	0.0206	0.53	0.608
Lighting	2	0.0611	0.0305	0.79	0.49
Number of passes	2	0.0770	0.0385	1.00	0.416

Table 11. Analysis of the levels of the parameters in the Buddha figure.

Level	Distance	Speed	Sensor Angle	Lighting	Passes
1	0.0983	0.2981	0.3236	0.3257	0.2362
2	0.2262	0.1972	0.2081	0.2705	0.3494
3	0.4556	0.2852	0.2485	0.1841	0.1945

The analysis of the results of the three objects enabled the definition of the following scanning parameter levels:

- Distance: Level 1 (0.5 m),
- Scanning speed: Level 3 (approximately 1.26 m/s)
- Sensor angle: No statistical significance was found for this parameter. It was fixed as Level 3 (variable).
- Lightning: Level 1 (natural lighting)
- Passes: No statistical significance was found for this parameter. It was fixed as Level 1 (one pass).

To verify the adequacy of the selected scanning parameters, a new scan of the three objects was conducted. The results of the scanned objects for the selected scanning parameters are illustrated in Figure 5. For each of these objects, the distance measurements were taken and the overall errors E_o were calculated. The obtained values of the three objects were 1.04%, 1.85%, and 0.96, respectively. The values of the obtained measurements in the digital models are summarized in Table 12.

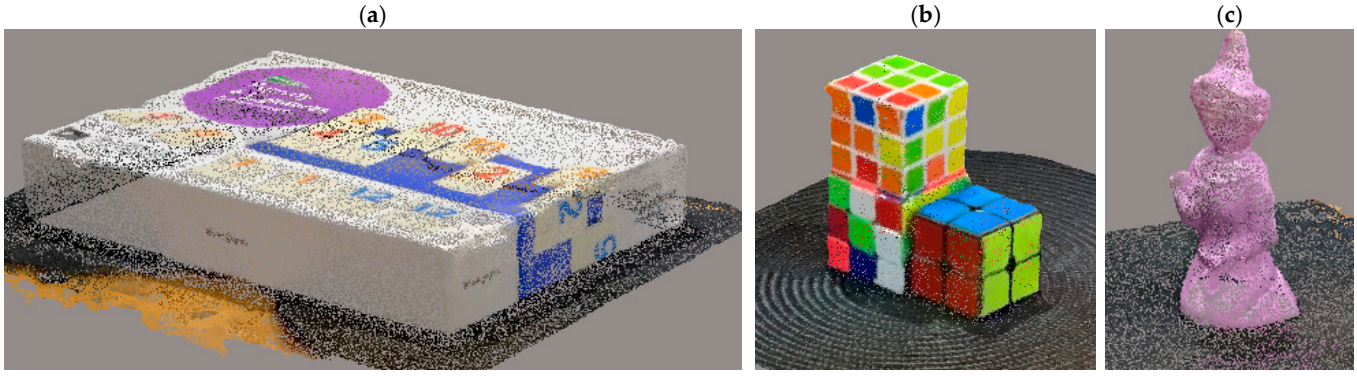


Figure 5. Scanned objects with the selected scanning parameters: (**a**) Parallelepiped Game Box, (**b**) Block of Kubik's cubes, and (**c**) Buddha shape sculpture.

Table 12. Dimensions measured in the objects scanned with the selected scanning parameters.

Object	Dimension 1	Dimension 2	Dimension 3
Parallelepiped Game box	a	b	c
	35.0	24.5	5.7
Rubik's cube block	l_1	l_2	l_3
	5.2	5.4	4.9
Buddha figure	h	m_1	m_2
	19.7	12.3	2.1

Figure 6 presents the E_o values from the 18 experiments (numbered from 1 to 18), along with the results from the scan using the selected scanning parameters (plotted as experiment number 19). Analysis of this figure shows that the resulting errors (1.043% for the Game box, 1.857% for the Rubik's cube, and 0.962% for the Buddha figure) were smaller than those observed in the other experiments analyzed.

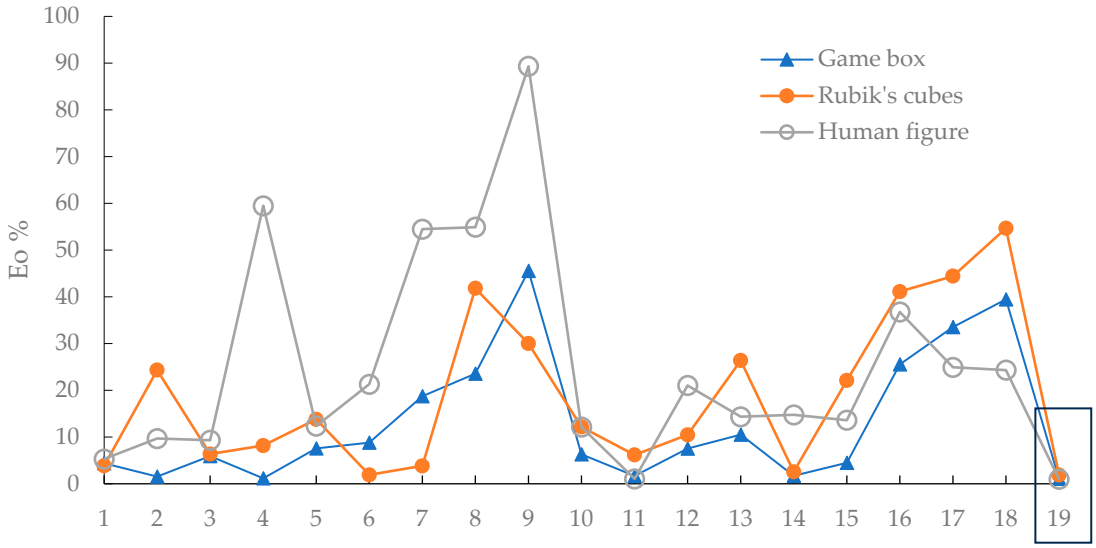


Figure 6. E_o values for the different experiments from the L18 and the scan with the selected scanning parameters (experiment 19 framed).

5. Case Study

The case study focuses on the Miguel Maraña gate of Santa Ana Church in Seville, Spain, presented in Figure 7. This door has a rich history and has undergone stratigraphic, typological, and construction analyses, as presented in [40]. This work explains that the wall's foundation dates back to the 12th century, the brick cladding to the 20th century, and the marble column to the 16th century. Throughout the door, several areas of damage were evident. Notably, there were long and narrow vertical openings resulting from the separation of the bricks.



Figure 7. Picture of the Miguel Maraña gate of Santa Ana Church.

This structure was scanned with the LiDAR of the iPad Pro fixing the scanning parameters with those levels defined in the preceding section—a distance of 0.5 m, scanning

speed of approximately 1.26 m/s, variable sensor angle, natural lighting, and one pass. The scanning was conducted on a sunny day, 26 June 2024, at 7:30 PM.

In order to validate the geometry of the model, the following reference distances (D) were defined: D_1: Horizontal measurement of a stone brick, D_2: Vertical measurement of a stone brick, D_3, Horizontal measurement of clay brick, D_4: Vertical distance of a first crack opening, and D_5: Vertical distance of a second crack opening. The values of these distances measured on site were: D_1 = 51.0 cm, D_2 = 29.0 cm, D_3 = 17.0 cm, D_4 = 58.4 cm, and D_5 = 38.2 cm, respectively. A picture of these considered distances in the model is presented in Figure 8.

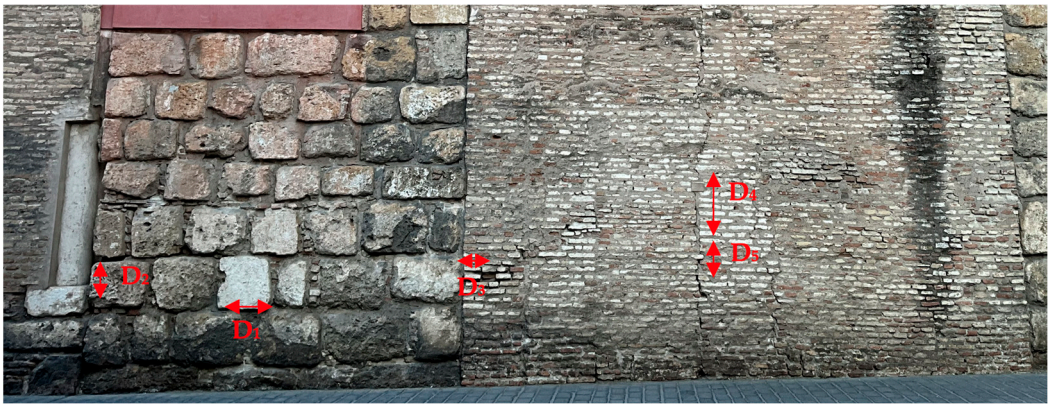


Figure 8. Considered referenced distances D in the case study.

The dimensions of the bricks were averaged across 10 different measurement points, using a steel tape measure with an accuracy of 1 mm. It is important to highlight the targeted measurement points were selected on those bricks that presented the most uniform dimensions.

Scans of two different areas of the door were performed. The digital models generated by the Polycam app are presented in Figures 9 and 10, respectively. The obtained values of D_1, D_2, D_3, D_4., and D_5 in these scanned walls are summarized in Table 12. This table also includes overall error (E_o) adapting equation 1 to five measurements. The obtained value of this parameter of 3.59% indicates a high level of accuracy in the scanned geometry.

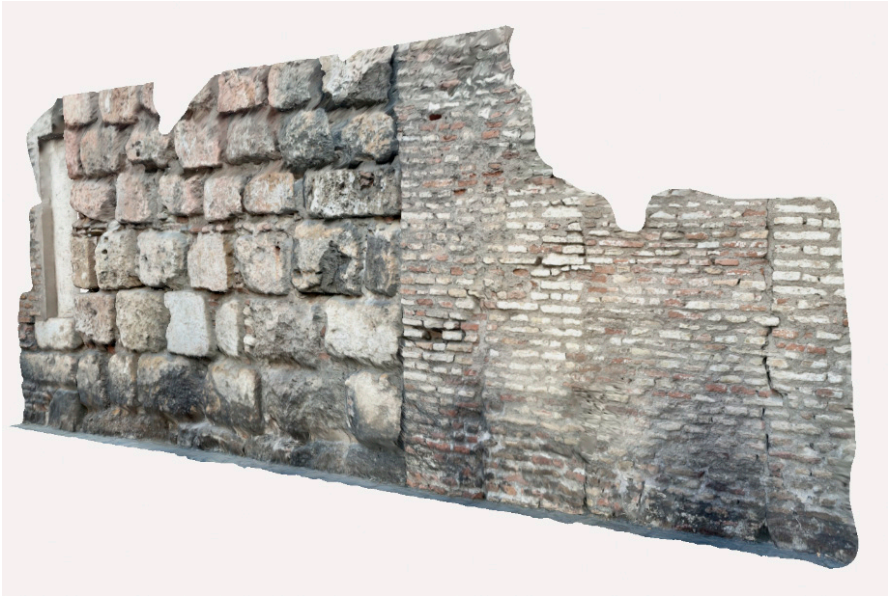


Figure 9. Scan 1: first area of the case study.



Figure 10. Scan of the second area of the case study.

To validate the positive impact of the selected scanning parameters, the case study was scanned using three alternative sets of parameters randomly chosen from the various levels studied. The values of the obtained measurements and the overall error (E_o) for these additional models are summarized in Table 13.

Table 13. Comparison of the values of the targeted measurements D and the Eo for the optimal scanning parameters and three random cases.

	D_1 (cm)	D_2 (cm)	D_3 (cm)	D_4 (cm)	D_5 (cm)	Eo %
Optimal parameters	47.5	28.5	16.0	57.6	39.1	3.6
Random parameters	44.8	26.6	11.2	64.6	39.5	13.7
	47.1	20.6	12.8	63.7	33.3	16.6
	49.6	21.8	18.9	64.6	46.9	14.4

To illustrate the variability in the five targeted measurements (D), a box-and-whisker diagram was created based on the measurements from the four scanners used for the structure. This diagram is presented in Figure 11. This diagram shows the variability in all the five targeted parameters due to the scanning parameters.

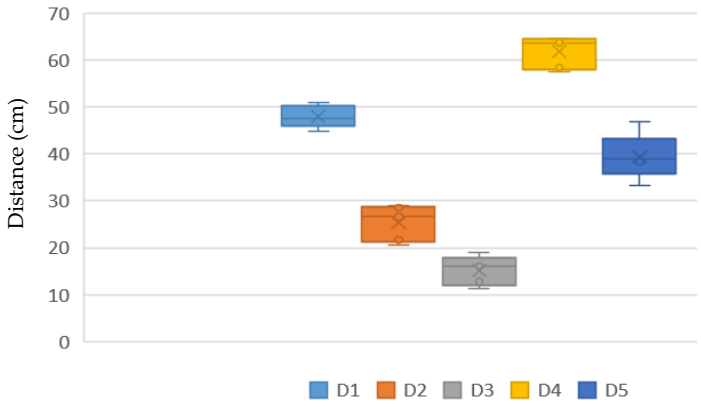


Figure 11. Box-and-whisker diagram of the targeted measurements D.

6. Discussion

For the case study, initially, a three-dimensional, full-scale sculpture with no straight lines was considered as the validation example. This choice posed challenges in measuring reference distances and underscored the importance of using volume as a reference. However, the sculpture was ultimately not selected, and a brick wall was chosen instead as the case study to more effectively demonstrate the connection between the proposed methodology and architectural applications. In this scenario, estimating the volume was not practical since the bricks were partially embedded within the wall, making reference distances a more suitable approach. For this reason, distances were ultimately selected over volume for the analysis.

This study addresses the limitations of iPad LiDAR for small, intricate cultural heritage artifacts, consistent with findings by Łabędź et al. [10], who highlighted its strength in capturing larger, simpler architectural features. The challenges stem from the sensor's resolution and the difficulty of maintaining optimal positioning during scans, as also noted by Teo and Yang (2023) [41], who recommend maintaining a consistent scanning distance and angle for improved accuracy. While initial tests used everyday objects for accessibility, future research will focus on cultural heritage specific artifacts, such as columns and façades, to refine the methodology. These adjustments aim to enhance the reliability and applicability of LiDAR-based documentation for heritage structures conservation.

The analysis of the models was intentionally kept as simple as possible to highlight the method's applicability and to encourage its use. As a result, the effects of converting the scan to a mesh, noise reduction algorithms, and potential data loss during the export/import process were not explored in this study. However, in future work, the proposed methodology will be extended to examine the potential effects of these parameters to enhance the robustness of the methodology and further explore its potential.

It is important to emphasize that the primary objective of this work is not to identify the software but rather to propose a methodology for analyzing the effects of scanning parameters across any given tools. Future research could build on this approach by incorporating the influence of software. This would involve introducing new parameters, such as LiDAR application and mesh generation software, with various levels (e.g., Agisoft Photoscan or Reality Capture) for each, within the Taguchi analysis framework. Such an analysis would extend the proposed methodology, not only to identify the optimal scanning parameters but also to determine the best combination of LiDAR and mesh generation software for each specific case study. Moreover, the proposed methodology is not limited to the iPad Pro LiDAR and can also be applied to other LiDAR devices and to alternative scanning technologies, such as photogrammetry or terrestrial laser scanners. The application of this methodology to these other techniques will be explored in future research.

Finally, the choice of measurement parameter does not affect the primary objective of the paper, which is to identify the optimal scanning parameters for a given tool and a specific parameter. In fact, the proposed methodology is highly versatile and can be directly applied to other scanning parameters, such as volumes and areas, allowing for broader applications across different measurement types. The analysis of other measurement types will be studied in future works.

7. Conclusions

This work illustrates the significant role that scanning parameters—such as scanning distance, speed, angle, number of passes, and lighting—play in the accuracy of scans conducted with the iPad Pro's LiDAR. Despite this importance, no systematic methodology for defining the optimal levels of these scanning parameters is presented in the literature. To address this gap, this study proposes the application of Taguchi's orthogonal arrays to identify the critical scanning parameters and their optimal levels.

The analysis of three objects with varying complexities revealed that the most important scanning parameters are a short distance from the object, have a fast scanning speed, and natural lighting. The selected optimal levels were then used to scan a heritage structure

featuring different structural elements and cracks. The results obtained from scanning this structure demonstrate how the chosen optimal levels for the scanning parameters significantly reduce measurement errors in the geometry of the scanned model compared to randomly defined parameters.

In terms of practical applications, the findings hold significant promise for conservation professionals and researchers who often face financial constraints. The use of easily accessible devices, such as the LiDAR of the iPad Pro, opens up new possibilities for institutions with limited resources to engage in high-quality documentation efforts.

However, the study is not without limitations. One major constraint is the iPad Pro's limited range and reduced accuracy when capturing complex geometries or finer details in intricate heritage structures. The LiDAR sensor's 5-m range and relatively low point density, especially compared to professional-grade terrestrial laser scanners, remain limitations that affect its ability to capture highly detailed or large-scale heritage elements. Additionally, environmental factors, such as lighting conditions and surface reflections, still pose challenges, which were controlled to some extent in this study but may not be easily manageable in all field conditions.

Future research should address these limitations by exploring improvements in both the hardware and software associated with mobile LiDAR technologies. Specifically, further studies could investigate enhanced calibration methods to optimize accuracy when scanning complex geometries and under varying environmental conditions. The integration of multi-sensor data fusion, combining LiDAR with photogrammetry or other technologies, could help overcome some of the inherent limitations of using a single scanning technique. Moreover, future studies could extend the scope of preliminary tests to include objects directly related to cultural heritage, such as architectural elements (e.g., columns, beams) and decorative artifacts. Focusing on these specific targets, the methodology will be better aligned with its intended applications in heritage conservation. In addition, future studies could extend this approach by incorporating the influence of different mesh generation software, introducing a new parameter (mesh software). This influence could potentially introduce data loss or distortions affecting the models' performance. Finally, testing the applicability of this technique in interdisciplinary contexts—such as archaeology or environmental monitoring—would expand the utility of mobile LiDAR scanning, offering further contributions to diverse fields that require affordable, accurate 3D documentation solutions.

Author Contributions: Conceptualization, E.A. and J.A.L.-G.; methodology, E.A., A.M. and J.A.L.-G.; software, E.A. and A.M.; validation, J.G.-A., A.M. and F.L.; formal analysis, E.A., A.M. and J.A.L.-G.; investigation, E.A., A.M., J.G.-A., F.L. and J.A.L.-G.; resources, J.G.-A.; data curation, E.A. and A.M.; writing—original draft preparation, E.A. and A.M.; writing—review and editing, J.G.-A., F.L. and J.A.L.-G.; supervision, J.A.L.-G.; funding acquisition, J.G.-A. All authors have read and agreed to the published version of the manuscript.

Funding: The authors are indebted to the project PID2021-126405OB-C32 funded by FEDER funds—A Way to Make Europe and Spanish Ministry of Economy and Competitiveness MICIN/AEI/10.13039/501100011033/. The financial support of the regional project SBPLY/23/180225/000113 funded by Junta de Comunidades de Castilla-La Mancha (Spain) is also greatly appreciated.

Institutional Review Board Statement: Not applicable.

Informed Consent Statement: Not applicable.

Data Availability Statement: The raw data supporting the conclusions of this article will be made available by the authors on request.

Conflicts of Interest: The authors declare no conflicts of interest.

References

1. Ricca, M.; La Russa, M.F. Challenges for the Protection of Underwater Cultural Heritage (Uch), from Waterlogged and Weathered Stone Materials to Conservation Strategies: An Overview. *Heritage* **2020**, *3*, 402–411. [CrossRef]
2. Haddad, N.A.; Fakhoury, L.A.; Sakr, Y.M. A Critical Anthology of International Charters, Conventions & Principles on Documentation of Cultural Heritage for Conservation, Monitoring & Management. *Mediterr. Archaeol. Archaeom.* **2021**, *21*, 291–310. [CrossRef]
3. Benchekroun, S.; Ullah, I.I.T. Preserving the Past for an Uncertain Future: Accessible, Low-Cost Methods for 3D Data Creation, Processing, and Dissemination in Digital Cultural Heritage Preservation. In Proceedings of the 26th International Conference on 3D Web Technology, Evry-Courcouronnes, France, 2–4 November 2022; Association for Computing Machinery: New York, NY, USA, 2022.
4. Alison, P.; Atencio, E.; Rivera, F.M. Calibration of UAV Flight Parameters to Inspect the Deterioration of Heritage Façades Using Orthogonal Arrays. *Sustainability* **2023**, *15*, 232. [CrossRef]
5. Atencio, E.; Muñoz, F.P.; Muñoz La-Rivera, F.; Lozano-galant, J.A. Calibration of UAV Flight Parameters for Pavement Pothole Detection Using Orthogonal Arrays. *Autom. Constr.* **2022**, *143*, 104545. [CrossRef]
6. Fangi, G. Spherical Photogrammetry for Cultural Heritage Metric Documentation: A Critical Review. In *Built Heritage: Monitoring Conservation Management*; Toniolo, L., Boriani, M., Guidi, G., Eds.; Springer International Publishing: Cham, Switzerland, 2015; pp. 301–311. ISBN 978-3-319-08533-3.
7. Westoby, M.J.; Brasington, J.; Glasser, N.F.; Hambrey, M.J.; Reynolds, J.M. "Structure-from-Motion" Photogrammetry: A Low-Cost, Effective Tool for Geoscience Applications. *Geomorphology* **2012**, *179*, 300–314. [CrossRef]
8. Gordon, M.; Batallé, A.; De Wolf, C.; Sollazzo, A.; Dubor, A.; Wang, T. Automating Building Element Detection for Deconstruction Planning and Material Reuse: A Case Study. *Autom. Constr.* **2023**, *146*, 104697. [CrossRef]
9. Teppati Losè, L.; Spreafico, A.; Chiabrando, F.; Giulio Tonolo, F. Apple LiDAR Sensor for 3D Surveying: Tests and Results in the Cultural Heritage Domain. *Remote Sens.* **2022**, *14*, 4157. [CrossRef]
10. Łabędź, P.; Skabek, K.; Ozimek, P.; Rola, D.; Ozimek, A.; Ostrowska, K. Accuracy Verification of Surface Models of Architectural Objects from the IPad LiDAR in the Context of Photogrammetry Methods. *Sensors* **2022**, *22*, 8504. [CrossRef]
11. Spreafico, A.; Chiabrando, F.; Teppati Losè, L.; Giulio Tonolo, F. The Ipad pro Built-in Lidar Sensor: 3D Rapid Mapping Tests and Quality Assessment. *Int. Arch. Photogramm. Remote Sens. Spat. Inf. Sci.-ISPRS Arch.* **2021**, *43*, 63–69. [CrossRef]
12. Çakir, G.Y.; Post, C.J.; Mikhailova, E.A.; Schlautman, M.A. 3D LiDAR Scanning of Urban Forest Structure Using a Consumer Tablet. *Urban Sci.* **2021**, *5*, 88. [CrossRef]
13. International Council on Monuments and Sites ICOMOS World Report 2000 on Monuments and Sites at Risk. Available online: https://www.icomos.org/public/risk/world_report/2000/trends_spa.htm (accessed on 15 October 2024).
14. Movilua, M.; Mihaela, G.; Olteanu-Donțov, I.; Banu, O.-M. Structural Rehabilitation of Historical Masonry Buildings. In *Proceedings of the Critical Thinking in the Sustainable Rehabilitation and Risk Management of the Built Environment*; Rotaru, A., Ed.; Springer International Publishing: Cham, Switzerland, 2021; pp. 587–599.
15. Yarzábal, L.A.; Buela, L.; de los Ríos, A.; Peláez, D.; Romero, M.; Espinoza, F.; Torres, A.S.; Medina, G.M.; Landi, J.G.; Tapia, M.V. Biological Deterioration of an Inca Monument at High Altitude in the Andean Range: A Case Study from Ingapirca's Temple of the Sun (Ecuador). *Heritage* **2022**, *5*, 2504–2518. [CrossRef]
16. Dashko, R.E.; Karpenko, A.G. Scientific-Practical Enhancement Principles for the Long-Term Stability of Cultural Heritage Objects through a Multi-Component Underground Space Analysis. *Heritage* **2024**, *7*, 4455–4471. [CrossRef]
17. De Fino, M.; Galantucci, R.A.; Fatiguso, F. Condition Assessment of Heritage Buildings via Photogrammetry: A Scoping Review from the Perspective of Decision Makers. *Heritage* **2023**, *6*, 7031–7066. [CrossRef]
18. Hull, J.; Ewart, I.J. Conservation Data Parameters for BIM-Enabled Heritage Asset Management. *Autom. Constr.* **2020**, *119*, 103333. [CrossRef]
19. de la Edificación, I.V. *Guía Para La Inspección y Evaluación Preliminar de Estructuras de Hormigón En Edificios Existentes*; Colegio Oficial de Arquitectos de Cádiz: Valencia, Spain, 2010.
20. Lozano, F.; Montalvo, A.; Porras, R.; Lozano-Galant, J.; Atencio, E. An Open-Source GIS App for Digitalizing Bridge Inspections and Automating BIM Model Integration. *Struct. Infrastruct. Eng.* 2024, *in press*.
21. Masciotta, M.G.; Morais, M.J.; Ramos, L.F.; Oliveira, D.V.; Sánchez-Aparicio, L.J.; González-Aguilera, D. A Digital-Based Integrated Methodology for the Preventive Conservation of Cultural Heritage: The Experience of HeritageCare Project. *Int. J. Archit. Herit.* **2021**, *15*, 844–863. [CrossRef]
22. Saisi, A.; Borlenghi, P.; Gentile, C. Between Safety and Conservation—Procedure for the Assessment of Heritage Buildings Based on Historic Research. *Buildings* **2023**, *13*, 2236. [CrossRef]
23. Adamopoulos, E.; Rinaudo, F. Close-Range Sensing and Data Fusion for Built Heritage Inspection and Monitoring—A Review. *Remote Sens.* **2021**, *13*, 3936. [CrossRef]
24. Costantino, D.; Vozza, G.; Pepe, M.; Alfio, V.S. Smartphone LiDAR Technologies for Surveying and Reality Modelling in Urban Scenarios: Evaluation Methods, Performance and Challenges. *Appl. Syst. Innov.* **2022**, *5*, 63. [CrossRef]
25. Díaz-Vilariño, L.; Tran, H.; Frías, E.; Balado, J.; Khoshelham, K. 3D Mapping of Indoor and Outdoor Environments Using Apple Smart Devices. *Int. Arch. Photogramm. Remote Sens. Spat. Inf. Sci.-ISPRS Arch.* **2022**, *43*, 303–308. [CrossRef]

26. Vogt, M.; Rips, A.; Emmelmann, C. Comparison of IPad Pro®'s LiDAR and TrueDepth Capabilities with an Industrial 3D Scanning Solution. *Technologies* **2021**, *9*, 25. [CrossRef]
27. Romero-Chambi, E.; Villarroel-Quezada, S.; Atencio, E.; Rivera, F.M. La Analysis of Optimal Flight Parameters of Unmanned Aerial Vehicles (UAVs) for Detecting Potholes in Pavements. *Appl. Sci.* **2020**, *10*, 4157. [CrossRef]
28. Vacca, G. 3D Survey with Apple LiDAR Sensor—Test and Assessment for Architectural and Cultural Heritage. *Heritage* **2023**, *6*, 1476–1501. [CrossRef]
29. Merchán, P.; Salamanca, S.; Merchán, M.J.; Pérez, E.; Moreno, M.D. Pasado, Presente y Futuro de Los HBIM (Heritage/Historic Building Information Models). In Proceedings of the XXXIX Jornadas de Automática, Badajoz, Spain, 5–7 September 2018; pp. 1077–1084. [CrossRef]
30. Hein, J.; Hippeli, J.; Eibert, T.F. Efficient EMC Parameter Analysis for the Verification of Complex Automotive Simulation Models by the Utilization of Design of Experiments. *IEEE Trans. Electromagn. Compat.* **2018**, *60*, 1965–1973. [CrossRef]
31. Kacker, R.N.; Lagergren, E.S.; Filliben, J.J. Taguchi's Orthogonal Arrays Are Classical Designs of Experiments. *J. Res. Natl. Inst. Stand. Technol.* **1991**, *96*, 577–591. [CrossRef]
32. Gisbert, C.M.; Lozano-Galant, J.A.; Paya-Zaforteza, I.; Turmo, J. Calibration of the Descent Local Search Algorithm Parameters Using Orthogonal Arrays. *Comput. Civ. Infrastruct. Eng.* **2020**, *35*, 997–1008. [CrossRef]
33. Peffers, K.; Tuunanen, T.; Rothenberger, M.A.; Chatterjee, S. A Design Science Research Methodology for Information Systems Research. *J. Manag. Inf. Syst.* **2007**, *24*, 45–77. [CrossRef]
34. Gonzalez-Lopez, F.; Bustos, G.; Munoz-Gama, J.; Sepúlveda, M. Domain Model Based Design of Business Process Architectures. *Appl. Sci.* **2022**, *12*, 2563. [CrossRef]
35. Atencio, E.; Mancini, M.; Bustos, G. Enterprise Architecture Approach for Project-Based Organizations Modeling, Design, and Analysis: An Ontology-Driven Tool Proposal. *Alex. Eng. J.* **2024**, *98*, 312–327. [CrossRef]
36. Atencio, E.; Araya, P.; Oyarce, F.; Herrera, R.F.; Muñoz-La Rivera, F.; Lozano-Galant, F. Towards the Integration and Automation of the Design Process for Domestic Drinking-Water and Sewerage Systems with BIM. *Appl. Sci.* **2022**, *12*, 9063. [CrossRef]
37. Polycam. Polycam. Available online: https://poly.cam/ (accessed on 4 November 2024).
38. Bentley. Bentley ITwin. Available online: https://www.bentley.com/software/itwin-capture-modeler/ (accessed on 4 November 2024).
39. Minitab Example of One-Way ANOVA. Available online: https://support.minitab.com/en-us/minitab/18/help-and-how-to/modeling-statistics/anova/how-to/one-way-anova/before-you-start/example/ (accessed on 4 November 2024).
40. Martínez Jordán, J.M. Estudio de Los Paramentos Del Alcázar de Sevilla: La Puerta Del León y La Puerta de Mañara. Master's Thesis, University of Sevilla, Seville, Spain, 2014.
41. Teo, T.A.; Yang, C.C. Evaluating the Accuracy and Quality of an IPad Pro's Built-in Lidar for 3D Indoor Mapping. *Dev. Built Environ.* **2023**, *14*, 100169. [CrossRef]

Disclaimer/Publisher's Note: The statements, opinions and data contained in all publications are solely those of the individual author(s) and contributor(s) and not of MDPI and/or the editor(s). MDPI and/or the editor(s) disclaim responsibility for any injury to people or property resulting from any ideas, methods, instructions or products referred to in the content.